COMPUTATIONAL PREDICTION OF THE RESISTANCE OF THE FLOATPLANE AT VARIOUS TRIM ANGLES

ARIES SULISETYONO, IHSAN FADHLURROHMAN

Department of Naval Architecture, Institut Teknologi Sepuluh Nopember, Surabaya, Indonesia
e-mail: sulisea@na.its.ac.id

BAHARUDDIN ALI

Balai Teknologi Hidrodinamika-BPPT Indonesia

ACHMAD ZUBAYDI

Department of Naval Architecture, Institut Teknologi Sepuluh Nopember, Surabaya, Indonesia

The prediction of the total resistance occurred during operation of a floatplane on the water surface is an important aspect in developing the floater as well as the engine power required. Theoretically, the trim angle of the floater may affect the total resistance. This paper intends to find the optimal trim angle for the take-off operation using the computational fluid dynamics (CFD) software. The floater set up under a fixed trim angle includes 2°, 5° and 10° taken in simulation at five different speeds between 9.21 m/s and 15.87 m/s. In one case of 2° trim angle, the floater model test has been carried out in a tow tank laboratory to validate the accuracy of the numerical result. Comparison of both results has a good fit with an average error of 2.27%. In the final simulation results, the optimum trim angle is 5°, which produces the total resistance less than 2° and 10° of the trim angle with average differences of 9.21% and 50.46% for all speeds, respectively.

Keywords: resistance, floatplane, trim angle, computational fluid dynamics

1. Introduction

Connectivity to all islands in an archipelago is very urgent in emergency situations such as natural disasters. A floatplane is the most suitable for passenger transportation, tourism purposes, rescue missions, disaster response measures, and could reach remote destinations (Qiu and Song, 2013). A floatplane is a seaplane that can take off and land on the water surface since it has a floater located under the fuselage like a boat functionally. The dynamic performances of the floater are generally the same as planing boats while running on seawater. When a floater moves forward, the longitudinal center of buoyancy (LCB) shifts backward increasing a water pressure at the bottom area of the after body. In a take-off operation, the speeds of a floatplane experience three stage conditions, namely displacement, plowing and planning. The displacement phase is a stage condition that the buoyancy force supports the total weight of the floater in the same position as the rest. The plowing phase is a condition when the hydrodynamic lift and buoyancy force support together the floatplane weight, and this gives the highest resistance. The planing phase is a condition when the entire weight of the floatplane is under support of the hydrodynamic lift of the floater and the aerodynamic lift of the wing. The planing phase generally occurs in high-speed floaters before take-off (FAA-H-8083-23, 2004).

It is important to minimize the resistance force making the floating aircraft take off in a short time period without requiring a high engine power, thereby reducing fuel consumption (Qiu and Song, 2013). The resistance force can be minimized by selecting some parameters such as principal dimensions, deadrise angle, transverse step, flare and trim angle at an early design

stage of the floater (Gudmundsson, 2014). The early studies have focused more on optimizing the floater trim angle to reduce the total resistance (Reichel *et al.*, 2014). Locke (1944) carried out a resistance test of flying boats in a tow tank laboratory to investigate the effect of the trim angle on the resistance force at the planing speed phase in the fixed-trim condition. And the test results concluded that the total resistance was influenced by the trim angles, and the optimal trim angle was between 5°-7° (Locke, 1944). The dynamic characteristics of the planing-tail were defined by Suydam (1952), namely the change in the trim angle of the planing-tail when operated in the plowing phase that showed a tendency to be more stable compared to a conventional planing boat. The floater trim angle is easy to change because of the transverse step located in the middle area of the longitudinal ship. However, the hull geometry could prevent the floater from experiencing a bigger change in the angle of balance during takeoff (Suydam, 1952). There is a strong correlation between the sternpost angle and the floater resistance while adjusting the correct sternpost angle to the non-submerged after the body has reduced the floater resistance (Gudmundsson, 2014). The highest resistance occured in the forebody area, and the resistance gradually decreased up to the transverse step area due to rotation of air in this area (Sazak, 2017). Sajedi and Ghadimi (2020) experimented on the double transversal step body in a high--speed boat with attention to decrease the total resistance compared to the non-transversal step body. In another work, the high deadrise angle in the forebody area could reduce the total resistance when the floater was moving forward at a speed before the planing phase (Sajedi and Ghadimi, 2020; Tomaszewski, 1950).

In principle, the floater resistance consists of two forms, namely friction and pressure resistances. The friction resistance arises because of viscosity or boundary layer thickness of a fluid, and the pressure resistance comes from the effect of the viscous fluid and waves that occur due to the shaped body (Molland *et al.*, 2017). The force components that act on the boat in the planing speed condition are hydrostatic and hydrodynamic forces in terms of the normal and tangential force. And the total resistance force consists of resistances due to the pressure force and the viscous force in the surface body (Savitsky, 1964). A floatplane commonly has two demihulls, which is called a catamaran. The interference of waves may occur in between the multihulls that may affect the resistance value. Insel and Molland (1992) introduced the total resistance formula of the catamaran, where the pressure field change around the hull, velocity augmentation between two hulls, and the wave resistance interference factor were accounted for including the form factor of the body.

In practice, the total resistance prediction of a ship is mostly obtained by the ship model test in the towing tank. Another approach to predict the resistance is to pursue numerical simulation by applying CFD techniques that enable low-cost research, guaranteeing high accuracy of the results compared to model testing. The 3D flow approach based on the Reynolds-averaged Navier-Stokes (RANS) equation under CFDSOF^{TM} v1.5 software was used to evaluate the total resistance of the floater catamaran pontoon of N219 Seaplanes (Yanuar *et al.*, 2020). The same approach using the volume of fluid (VOF) method considering the free surface elevation was successfully applied to simulate the porpoising phenomenon of the floater (Alifrananda *et al.*, 2022). The interface between the solid hull and the fluid boundaries was under evaluation by the fractional area volume representation method (Berg, 2015; Versteeg and Malalasekera, 2007).

2. Methodology

The floater design of the lines plan which includes the body, sheer and half-breadth plans are shown in Figs. 1, 2, and 3, respectively (Alifrananda and Sulisetyono, 2021). The floater body type is a double hull or catamaran with principal dimensions as described in Table 1.
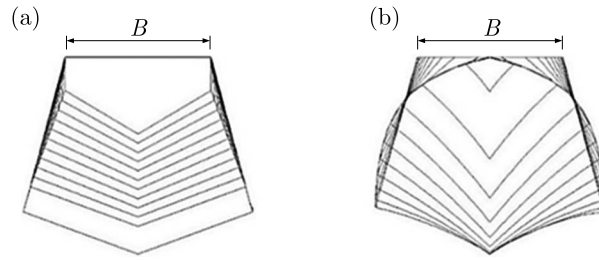
Fig. 1. Body plan of the floater: (a) after body, (b) fore body
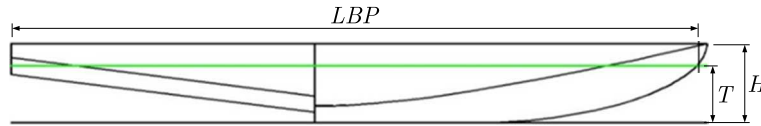
Fig. 2. Sheer plan of the floater
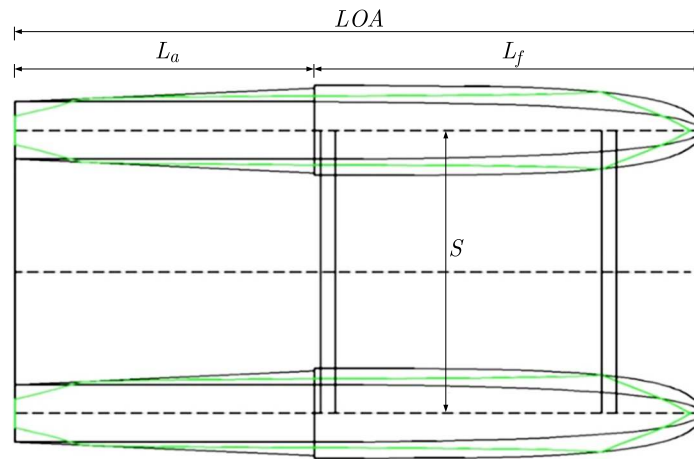
Fig. 3. Half-breadth plan of the floater

Table 1. Principal dimensions of the floater prototype

Parameter	Prototype
Length overall (LOA)	9.40 m
Length between perpendiculars (LBP)	9.27 m
Breadth of demihull (B)	1.25 m
Height (H)	1.07 m
Draught (T)	0.77 m
Space between demihulls (S)	3.95 m
Forebody length (L_f)	5.30 m
Afterbody length (L_a)	4.10 m
Displacement (Δ)	7.33 ton

The trim is set up to 2°, 5°, and 10° of angles by rotating the floater hull at the point center as presented in Figs. 4, 5, and 6, respectively. In this case, the displacement of the three model cases are approximately the same or about 0.5% of the maximum difference. The center of rotation is also identified as the center of gravity of the floater hull located 4.6 m forward the after perpendicular (AP) and 0.69 m above the keel, where the point is close to the transverse step location of the floater hull. The center point of buoyancy shifts because of the wetted body

area change after the increased trim angle. Length between perpendiculars (LBP) becomes short due to the trim of the body as presented in Figs. 4, 5 and 6. The principal dimensions of model cases A, B and C are described in Table 2.
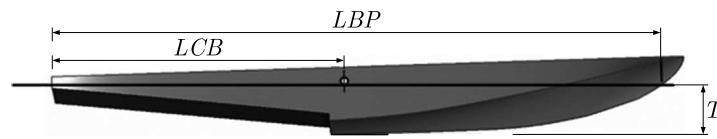
Fig. 4. Floater model case A (trim angle = 2°)
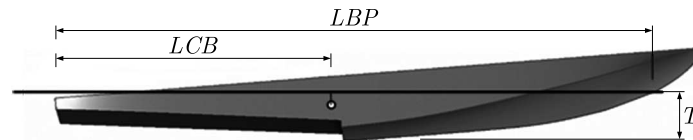
Fig. 5. Floater model case B (trim angle = 5°)
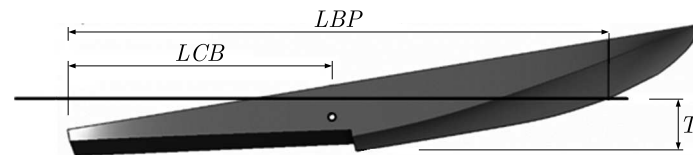
Fig. 6. Floater model case C (trim angle = 10°)

Table 2. Hydrostatics of the varied model cases

Dimensions	Unit	Model		
		case A	case B	case C
Trim angle	deg	2	5	10
Length between perpendiculars (LBP)	m	9.02	8.59	7.90
Breadth of demihull (B)	m	1.25	1.25	1.25
Draught (T)	m	0.78	0.79	0.86
Displacement (Δ)	ton	3.50	3.49	3.48
Longitudinal center of buoyancy (LCB)	m	4.42	3.77	3.25

The setting of CFD simulation is adjusted to refer to the experiment setup in which the floater is pulled at a fixed-trim angle. In this study, the lift force of the floater is neglected because it is not sufficient to lift the aircraft body weight. This assumption may acceptable since the study considers only the trim angle effect (Locke, 1944). However, the trim angle of the planing-tail floater during the plowing position tends to be stable (Gudmundsson, 2014). With such characteristics, the floater resistance evaluation could be simplified by testing the fixed-trim resistance (Locke, 1944). The CFD setup is examined with comparison between the numerical results and the model tested for the trim angle case of 2°. Figure 7 shows the model test which is carried out in the towing tank laboratory of LHI in Indonesia. The model test has dimensions with a scale of 1:9.40 to the prototype, namely length overall (LOA) 100 cm, breadth of demihull (B) 13.3 cm, draught (T) 8.2 cm, and space between demihulls (S) 42 cm.

In general, three processes of CFD simulation are defined such as pre-processor, solver, and post processor. The pre-processor consists of the modelling process and grid generation in the CFD software. The fluid domain boundary is created refering to the International Towing Tank Conference recommendations regarding the good domain boundary sizes (ITTC, 2011) to be successfully applied into the resistance simulation in the case of MOERI Container Ship (Sherbaz
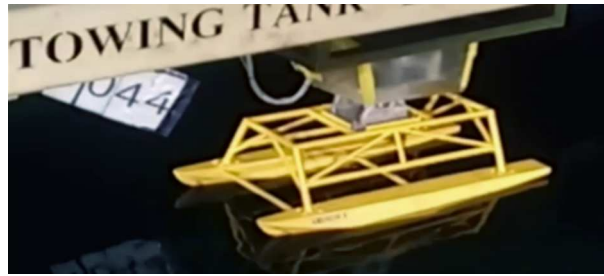
Fig. 7. Floater model test in the towing tank laboratory of LHI

and Duan, 2014), and KCS (ITTC, 2011). Domain boundaries generally consist of upstream, downstream, side, bottom and top parts. The upstream boundary distance from the bow of the floater is approximately $1LBP$ (length between perpendiculars), the downstream distance from the stern is approximately $2LBP$, the side boundary distance from the plane of symmetry is about $1LBP$, the bottom boundary distance is approximately $1\ LBP$, and the top boundary distance is approximately $1LBP$ from the keel (ITTC, 2011). The domain boundary conditions are created for the condition of two hulls which are intended to experience the interaction between them based on the shape of the water surface. The illustration of the domain boundary set-up of the CFD simulation is shown in Fig. 8.
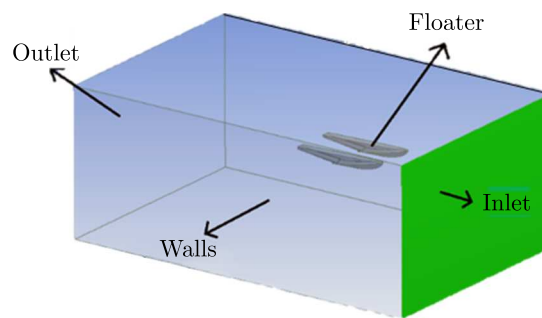
Fig. 8. Boundary domain set up
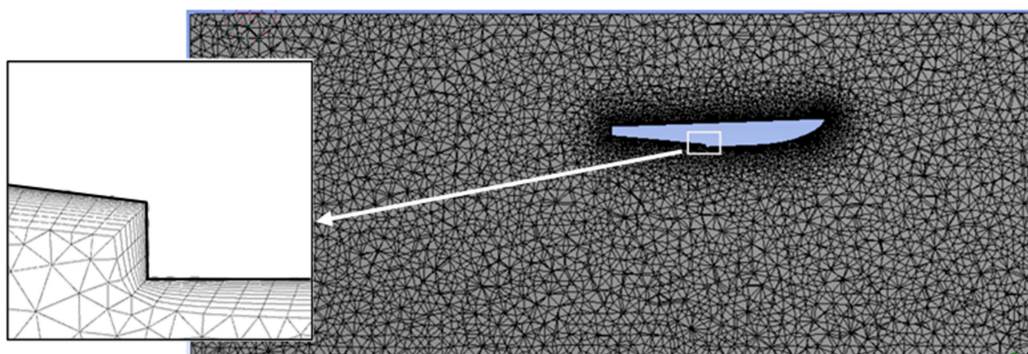
Fig. 9. Grid generation

The grid or mesh generation across the fluid domain consists of several elements in which the grid size influences the mesh number. A high number mesh can provide better accuracy of the simulation result even the time simulation spent is getting longer. On the contrary, fewer meshes make the result less accurate but faster in simulation time. Therefore, it is necessary to study the independence of the mesh to get an optimal number of meshes for simulation. In the mesh generation, the element shape is like a tetrahedral located in the fluid area outside the

floater hull. Face sizing is adopted to make the mesh around the floater hull more compact to estimate the forces acting around the floater hull more accurately. The inflation layer used is to make prisms or structured nets around the surface of the floater hull and the mesh refinement at the free surface area around the hulls as presented in Fig. 9. The way to find the optimum mesh is, by comparison, the current simulation result with the previous step results, and if the margin of both the results is less than 2% as a requirement, then the mesh number is independent. In general, the CFD setting in the post-processor includes the transient speed, fluid modeling in two phases, implicit body force and the turbulence k-ω SST model. The turbulence model has a coefficient of resistance close to the actual value and provides clear flow separation. The solution uses a simple scheme, the presto pressure, and the compressive fraction volume.

Numerical simulation performances are under fixed trim conditions of $2°$, $5°$ and $10°$ at five speed variations such as $9.21\,\mathrm{m/s}$, $10.65\,\mathrm{m/s}$, $12.38\,\mathrm{m/s}$, $14.11\,\mathrm{m/s}$, and $15.85\,\mathrm{m/s}$ which are adjusted as the speed in the floater plowing phase. In this phase, the friction resistance generally reaches its peak before the floatplane experiences the planing phase position. The total resistance that occurs at that time R_T is defined by the CFD simulation as well as the model test, and the total resistance coefficient C_T is obtained as

$$C_T = \frac{2R_T}{\rho S v^2} \tag{2.1}$$

where ρ is density of seawater, S is the wetted surface area of the hull, and v is velocity, m/s. For the analysis purposes, the total resistance is plotted as a function of the speed coefficient C_v obtained by

$$C_v = \frac{v}{\sqrt{g^B}} \tag{2.2}$$

3. Results and discussion

It is found from the grid independence study that the optimum number of elements is about 1,230,518 with the size of $y+150$ units when the force coefficient margin between step 4 and 5 of simulation is about 1.85%, as shown in Fig. 10. The validation process is needed to ensure the computational setup on the CFD software to meet good accuracy and avoid computational errors. The validation procedure is made by comparing the results of CFD simulations with the model test results performed in the towing tank laboratory. The requirement is that the results of the CFD simulation are to be validated if the comparison margin is less than 5%. Figure 11 shows the comparison between both results. In the validation case, the simulation takes the floater trim angle of $2°$ (model case A) at a speed coefficient of 1.86 to 3.20. The highest margin occurs at the speed coefficient of 3.20 and is about 4.07% or less than 5%, and the margin average about 2.27%. So that the CFD setup is valid to be used further for other trim angle cases.

The coefficient of resistance forces acting on the floater hull in variations of the trim angle as a function of the speed coefficient C_v are described in Fig. 12. Figure 12 shows that the trim angles affect the total resistance of the floatplane significantly. For example, the model with a $5°$ of the trim angle (model case B) provides the lowest resistance, and the model with a trim angle of $10°$ (model case C) produces the highest resistance. These CFD results are like the model test results conducted by Locke (1944) on a similar model of aircraft but with different trim angles such as $4°$, $6°$, $8°$ and $10°$ at a high speed. The trim angle of $6°$ gives the smallest resistance value, and the highest resistance occurrs at a trim angle of $10°$ (Locke, 1944).
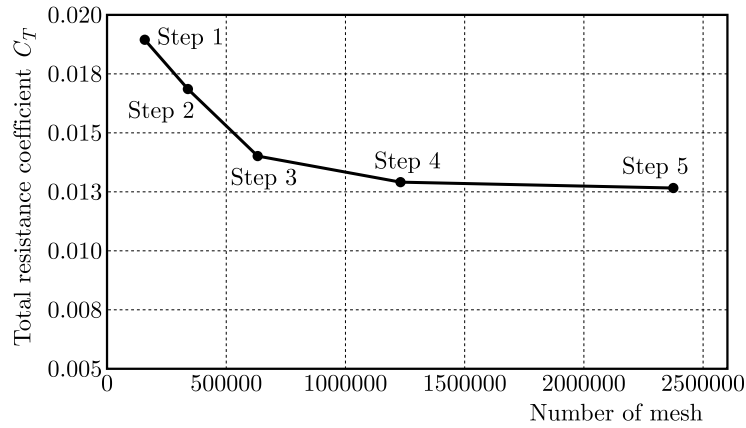
Fig. 10. Grid independence study
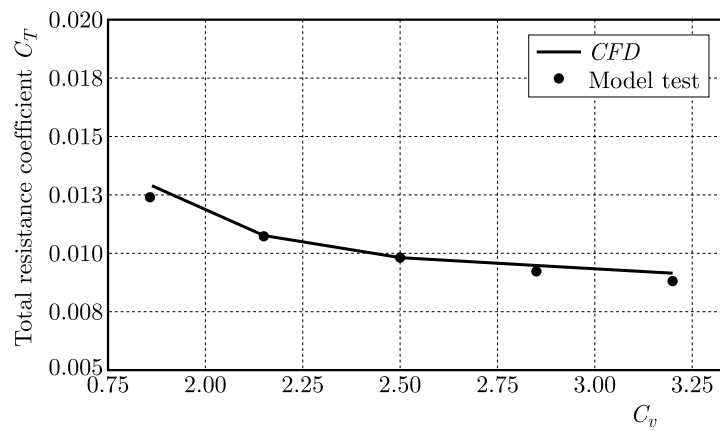
Fig. 11. Comparison of the CFD and model test results at the trim angle of 2°
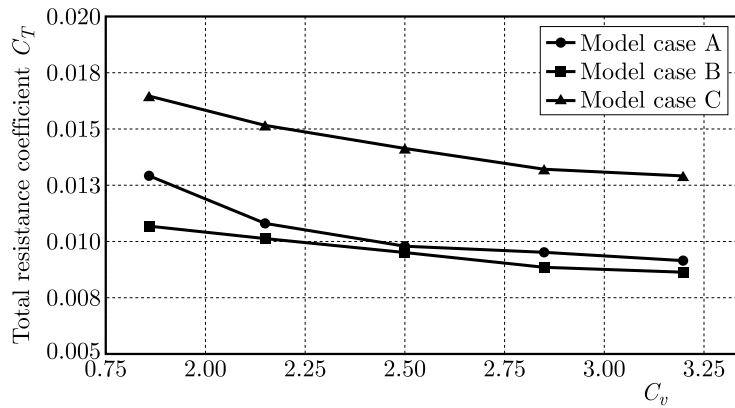
Fig. 12. Total resistance coefficient of the floater at various trim angles

Figure 13 explains that the total resistance of the floater decreases by about 7.22% while at trim angles in between 2° and 5°. However, at the angles between 5° and 10°, the total resistance of the floater increases by about 33.7%. And the trim angle of 5° (model case B) is the most optimum one because it gives the smallest total resistance for all speeds. It is shown in Fig. 13 that the total resistance increases at increasing speed for all trim angles, and the greatest total resistance is at the trim angle of 10° (model case C). In addition, the total resistance starts to increase exponentially at trim angles greater than 5°. The simulation results also present the

static pressure on the hull surface, the water volume fraction distribution, and the free surface wave pattern on the side and after the body.
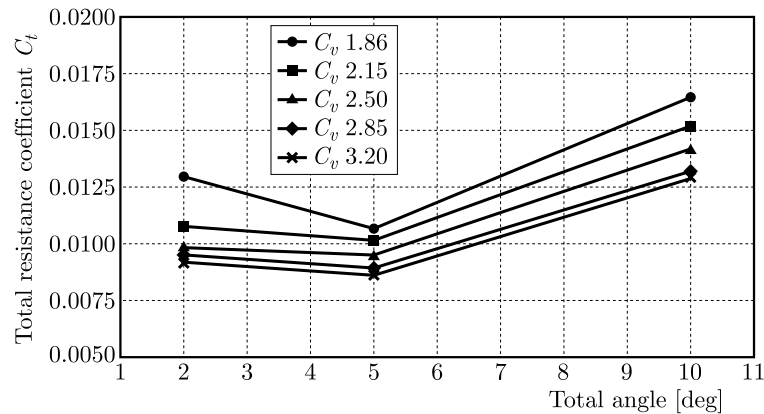
Fig. 13. Effect of trim angle to total resistance

Figures 14 and 15 show the distribution of static pressure acting on the hull surface in all model cases at the speed coefficient $C_v = 1.86$ and 3.2, respectively. All model cases show the highest static pressure pointed to the bow area with the order of leading model case A then followed sequentially by model case B and C because of differences in the trim angle. The highest static pressures as shown in Fig. 15 are about 18.43 kPa, 15.28 kPa and 14.21 kPa in model cases A, B and C, respectively. At the speed coefficient 3.2, the static pressures increase by about 48.24 kPa, 46.10 kPa, 48.75 kPa for model case A, B and C, respectively, see Fig. 16. However, the lowest static pressure appears in the area after the stepped hull as shown in Figs. 15 and 16. Static pressure in each model is correlated with the resistance value as Savitsky (1964) stated that the planing boat resistance consisted of the normal force and friction on the wetted surface of the hull.
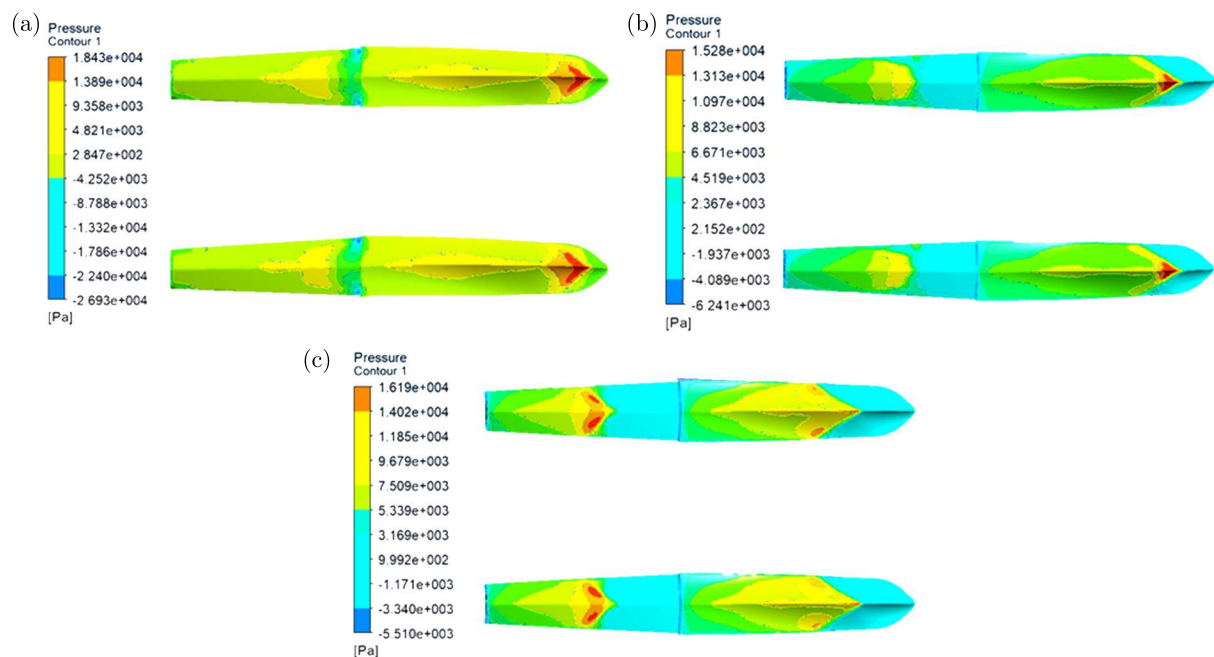
Fig. 14. Static pressure in (a) model A, (b) model B and (c) model C at $C_v = 1.86$
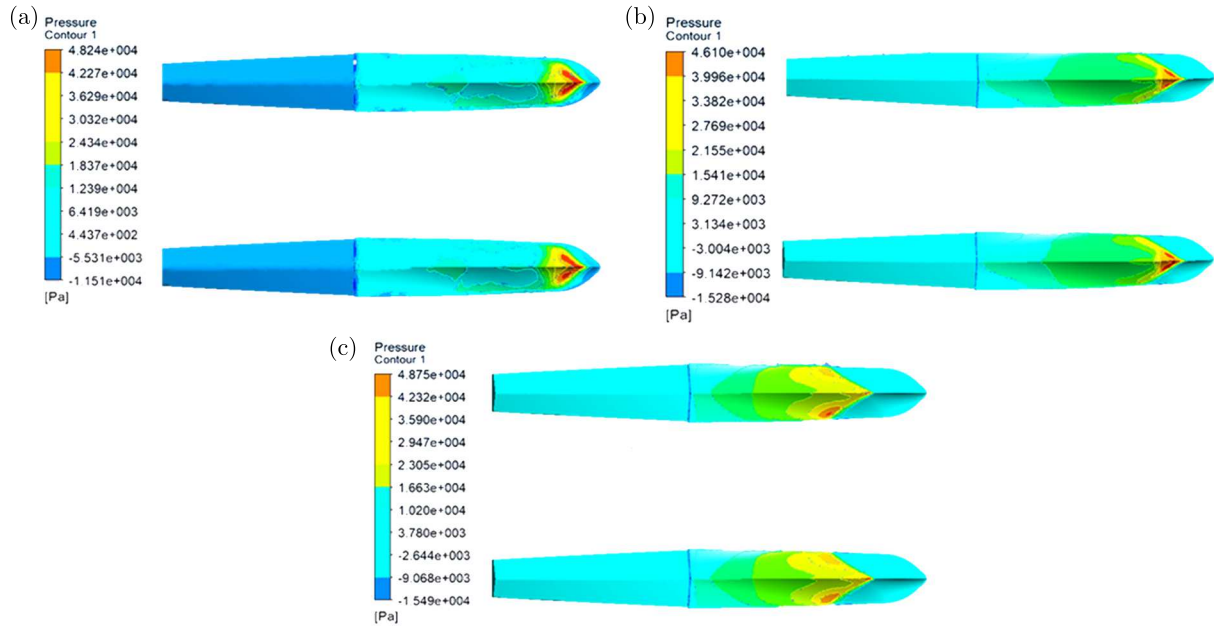
Fig. 15. Static pressure in (a) model A, (b) model B and (c) model C at $C_v = 3.2$

Figures 16 and 17 show the water volume fraction on the surface model case A, B and C at the speed coefficient C_v of 1.86 and 3.20, respectively. Volume fractions represent the space occupied by the water phase where the red and blue colors show the highest and lowest fraction of the water on the surface of the hull. Table 4 shows the area of highest water fraction (red color) that are measured using AutoCAD from the contour of Figs. 16 and 17, manually. In all model cases, the water volume fraction area tends to decrease while the speed of the floater increases. Model case C has the smallest water fraction area compared to other two model cases. Generally, the friction resistance is directly proportional to the water volume fraction area of the hull. However, the resistance is also affected by the viscous pressure acting on the body surface. Sum of the friction and viscous pressure resistances is called the viscous resistance as explained in Eq. (2.2), and the form factors of model cases A, B and C have differences due to the trim angle. Figures 14, 15, 16 and 17 also give confirmation that the highest static pressure area is at the same location as the highest intensity of the water volume fraction area.

Table 4. Water volume fraction of the floater

	Water volume fraction [m^2]		
C_v	Model case A	Model case B	Model case C
1.86	28.51	21.25	19.94
3.20	16.90	13.34	11.76

The free surface is defined as the boundary between two fluids, the water and the air. The floater moving forward on calm water may generate wave surface. The patterns of the generated wave are different in each model case as presented in Figs. 18 and 19 at a low speed of $C_v = 1.86$ and a high speed of $C_v = 3.2$, respectively. The red and blue colors indicate the highest and the lowest wave surface elevation, respectively. The highest wave occurring after the floater in model cases A, B and C at a speed coefficient 1.86 is about 1.19 m, 1.32 m, and 1.24 m, respectively. When the speed coefficient raises up to 3.2, the highest wave generated by the floater increases by about 1.36 m, 1.54 m and 1.81 m if model cases A, B and C, respectively.

The generated wave starts at the forward point of the model cases then flowd backward alongside of the hull. The wave interference occurs between the area of the floater demihulls,
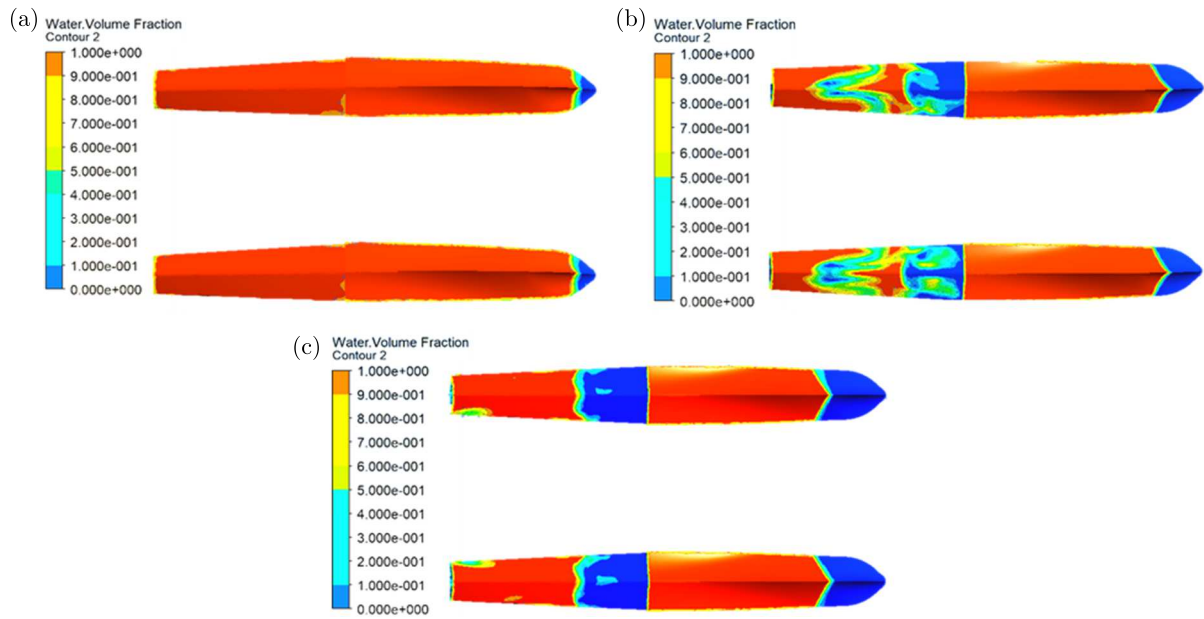
Fig. 16. Water volume fraction in (a) model A, (b) model B and (c) model C at $C_v = 1.86$
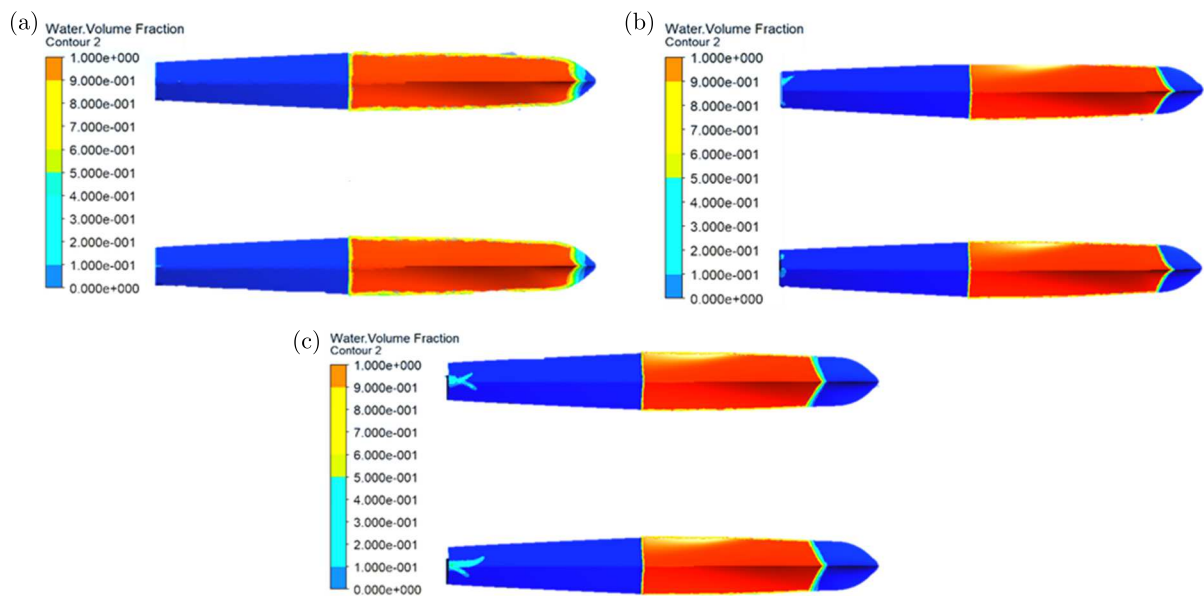
Fig. 17. Water volume fraction in (a) model A, (b) model B and (c) model C at $C_v = 3.2$

and this phenomenon produces additional resistance, namely, wave-making resistance. The characteristic of wave interference in the inter-demi-hull depends on the ratio of the space between demihulls S and the length of the waterline (LBP). Tables 1 and 2 show that S/LBP ratios in model cases A, B and C are about 0.44, 0.46 and 0.50, respectively. The ratio difference is due to decreasing of LBP while the trim angle increases. Figures 16, 17, 18 and 19 basically confirm the total resistance components which are the viscous resistance and the wave making resistance always fluctuating with the speed forward of the floater. In general, at a low speed of $C_v = 1.86$, the viscous resistance of all model cases may tend to be higher than at a high speed of $C_v = 3.2$, but the wave making resistance may look greater at a high-speed of $C_v = 32$, than at a low speed of $C_v = 1.86$.
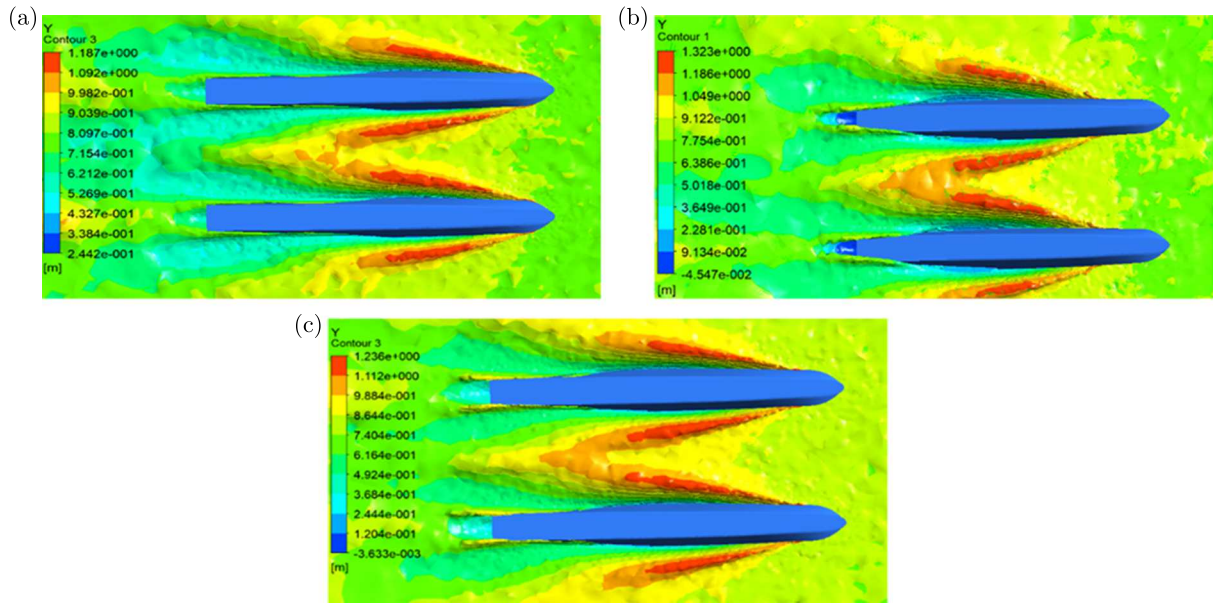
Fig. 18. Free surface pattern of (a) model A, (b) model B and (c) model C at $C_v = 1.86$
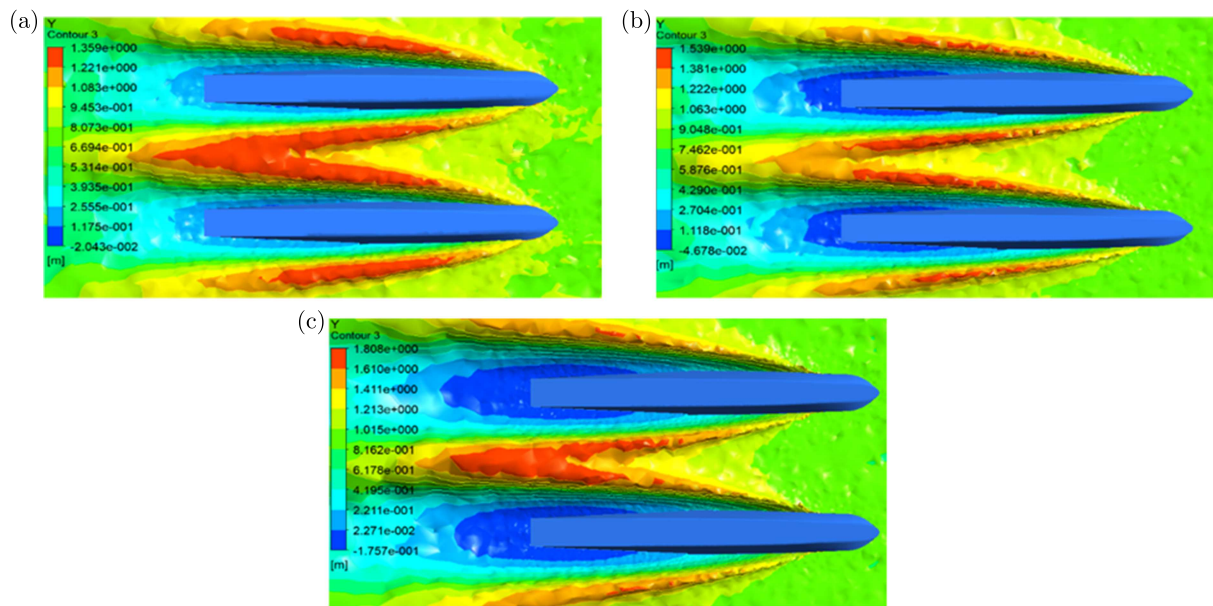
Fig. 19. Free surface pattern of (a) model A, (b) model B and (c) model C at $C_v = 3.2$

4.   Conclusions

The paper analyzes evaluation of the total resistance of the floater with trim angle variations at the speed of the plowing phase using the fluid dynamics software FLUENT. The three trim angles of the floater are 2°, 5° and 10°, are assumed to be fixed. They are simulated at the forward-moving body with the speed coefficients C_v of 1.86, 2.15, 2.50, 2.85 and 3.20. Testing results of the floater model in the towing tank are used to check the computational accuracy for the case of trim angle 2° with a conclusion that an average difference is about 2.27%. The CFD result explains that the trim model of 5° (model case B) generates a smaller total resistance for all speeds than in the models with the trim angles of 2° (model case A) and 10° (model case C) with an average difference of 9.21% and 50.46%, respectively.

References

1. ALIFFRANANDA M.H., SULISETYONO A., 2021, Porpoising instability study of the floatplane during take-off operation on calm water, *IOP Conference Series Materials Science and Engineering*, **1052**, 1, 012013

2. ALIFFRANANDA M.H., SULISETYONO A., HERMAWAN Y.A., ZUBAYDI A., 2022, Numerical analysis of floatplane porpoising instability at calm water during take-off, *International Journal Technology*, **13**, 1, 190-201

3. BERG T., 2015, Simulating sinkage & trim for planing boat hulls, *FLUENT Workshop*

4. Federal Aviation Administration (FAA-H-8083-23), 2004, *Seaplane, Skiplane, and Float/Ski Equipped Helicopter Operations Handbook*, Aviation Supplies & Academics Inc.

5. GUDMUNDSSON S., 2014, *General Aviation Aircraft Design*, Oxford: Elsevier

6. INSEL M., MOLLAND A.F., 1992, An investigation into the resistance components of high-speed displacement catamarans, *Transactions of the RINA*, **134**, 1-20

7. ITTC, 2011, Practical guidelines for ship CFD applications, 26th International Towing Tank Conference Specialist Committee on CFD in Marine Hydrodynamics.

8. LOCKE F.W.S., 1944, *General Resistance Tests on Flying-Boat Hull Models*, National Advisory Committee for Aeronautics, Wartime Report, NACA, Washington

9. MOLLAND A.F., TURNOCK S.R., HUDSON D.A., 2017, *Ship Resistance and Propulsion*, Cambridge University Press

10. QIU L., SONG W., 2013, Efficient decoupled hydrodynamic and aerodynamic analysis of amphibious aircraft water takeoff process, *Journal of Aircraft*, **50**, 5, 1369-1379

11. REICHEL M., MINCHEV A., LARSEN N.L., 2014, Trim optimization – theory and practice, *International Journal on Marine Navigation and Safety of Sea Transportation*, **8**, 3, 387-392

12. SAJEDI S.M., GHADIMI P., 2020, Experimental and numerical investigation of stepped planing hulls in finding an optimized step location and analysis of its porpoising phenomenon, *Mathematical Problems in Engineering*, **2020**

13. SAZAK E., 2017, *Parametric Investigation of Hull Shaped Fuselage for Amphibious UAV*, Middle East Technical University

14. SAVITSKY D., 1964, Hydrodynamic design of planing hulls, *Marine Technology*, **1**, 4, 71-95

15. SHERBAZ S., DUAN W., 2014, Ship trim optimization: assessment of influence of trim on resistance of MOERI container ship, *The Scientific World Journal*, **2014**

16. SUYDAM H.B., 1952, *Hydrodynamic Characteristics of a Low-Drag, Planing-Tail Flying-Boat Hull*, National Advisory Committee for Aeronautics, Washington

17. TOMASZEWSKI K.M., 1950, *Hydrodynamic Design of Seaplane Floats*, Aeronautical Research Council, Ministry of Supply, London

18. VERSTEEG H., MALALASEKERA W., 2007, *An Introduction to Computational Fluid Dynamics the Finite Volume Method*, Pearson Education Limited

19. YANUAR, GUNAWAN, UTOMO A.S.A., LUTHFI M.N., BAEZAL M.A.B., MAJID F.R.S., CHAIRUNISA Z., 2020, Numerical and experimental analysis of total hull resistance on floating catamaran pontoon for N219 seaplanes based on biomimetics design with clearance configuration, *International Journal of Technology*, **11**, 7, 1397-1405